A novel nonintrusive method to resolve the thermal dome effect of pyranometers: Instrumentation and observational basis

Qiang Ji[1,2] and Si-Chee Tsay[2]

Received 2 November 2009; revised 4 May 2010; accepted 27 May 2010; published 9 October 2010.

[1] A new method for improving the ground-based pyranometer measurements of solar irradiance has been employed during the East Asian Study of Tropospheric Aerosols and Impact on Regional Climate field experiment, Asian Monsoon Year in China in 2008. Depending on the temperature difference between its detector and domes, a pyranometer's thermal dome effect (TDE) can vary from a few W m^{-2} at night to over tens of W m^{-2} during daytime. Yet in traditional calibration procedures only a single calibration constant is determined, and consequently TDE is misrepresented. None of the methods that have been documented in the literature can capture TDE nonintrusively using the same instrument. For example, although adding a temperature sensor to the detector assembly is straightforward, attaching any sensor on a dome is intrusive and will affect its overall optical and physical properties. Furthermore, in response to the solar elevation and atmospheric variables, the dome temperature distribution is both dynamic and uneven, which makes it exceedingly difficult for locating a representative point on the dome for measuring TDE. However, the effective-dome-temperature is proportional to the pressure of the air trapped between the outer and the inner domes; therefore with a minor modification to a pyranometer, we can utilize the ideal gas law to gauge TDE without affecting the domes. Pyranometers can become climate-quality instruments once their TDE are nonintrusively determined.

Citation: Ji, Q., and S.-C. Tsay (2010), A novel nonintrusive method to resolve the thermal dome effect of pyranometers: Instrumentation and observational basis, *J. Geophys. Res.*, *115*, D00K21, doi:10.1029/2009JD013483.

1. Introduction

[2] Climate studies require long-term accurate observations of solar and terrestrial irradiances (fluxes) at the Earth's surface. Commercial pyranometers, such as the Eppley Precision Spectral Pyranometer, have been widely used since the 1950s for measuring solar irradiance. However, until recently a major uncertainty in pyranometer specification is identified as the "zero (or thermal) offset," which is not a random error. Note that for any high-quality (or suitable for use as a working standard) pyranometer [see *World Meteorological Organization*, 2008, Table 7.5], this offset is currently tolerated to as large as 7 W m^{-2} in response to 200 W m^{-2} net thermal radiation under ventilated conditions, plus ±2 W m^{-2} in response to a 5 K h^{-1} change in ambient temperature. Although it was believed that the zero offset is related to the thermal emission of the instrument's two glass domes, in earlier studies it was either ignored, approximated as a constant, or crudely treated [e.g., *Gulbrandsen*, 1978], because of lacking a theoretical explanation. Depending on how a pyranometer is calibrated [e.g., *Dutton et al.*, 2001; *Philipona*, 2002; *Michalsky et al.*, 2003; *Reda et al.*, 2003; *Ji*, 2007], ignoring this thermal dome effect (TDE) can cause a few percent of uncertainty in the measurement results; and its consequences are not limited to the surface, because the surface flux is related to the radiative transfer in the whole column of atmosphere. As a variable that depends on environmental conditions, the uncertainty in TDE, even on a daily or monthly average, are comparable to or larger than the < 2 W m^{-2} level of radiative effect considered important in climate studies [*Intergovernmental Panel on Climate Change*, 2007].

[3] The TDE should be carefully considered in any studies of atmospheric energetics, in particular when seemingly inexplicable anomalies are found [e.g., *Stephens and Tsay*, 1990]. In some recent investigations [e.g., *Bush et al.*, 2000; *Haeffelin et al.*, 2001] thermistors were attached onto the outer or the inner dome of a pyranometer for measuring the dome temperature, which verified a theoretical explanation of TDE. Unfortunately, attaching a sensor on a transparent glass dome can alter the optical and thermal properties of the instrument: first, the sensor and its wires are inside the field of view of the instrument's detector, causing interference; second, a sensor itself is directly heated by sunlight, biasing the measurement; third, the temperature distribution on the dome can be disturbed by objects attached to the dome, altering the outcome. Most importantly, the dome's dynamic

[1]ESSIC, University of Maryland, College Park, College Park, Maryland, USA.
[2]Laboratory for Atmospheres, NASA Goddard Space Flight Center, Greenbelt, Maryland, USA.

Copyright 2010 by the American Geophysical Union.
0148-0227/10/2009JD013483

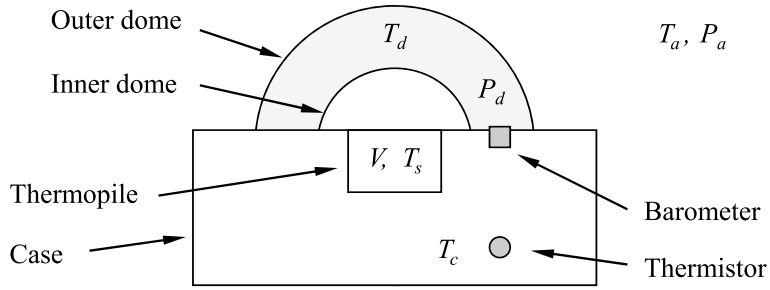

Figure 1. Schematic of a modified pyranometer where the ideal gas law is employed to relate the measured pressure of the sealed space between the inner and outer domes (P_d) and the effective dome temperature (T_d). See section 2 for details.

temperature field is far from uniform, and it changes with the position of the sun, distribution of clouds, wind speed, and other atmospheric conditions. Therefore there is no ideal place to attach a sensor to best represent TDE at all times.

[4] In this paper we (1) present an innovative technique to quantify the effective-dome-temperature without disturbing the proper function of the domes, (2) demonstrate a method that incorporates the information obtained from the technique to differentiate TDE, based on partitioning the pyranometer measurements explicitly, and (3) discuss some characteristics of TDE and potential applications of the new method. In short, this paper is intended to demonstrate the new method's instrumentation and observational basis. Applications such as analysis of the surface radiative energetics during our deployment of Asian Monsoon Year 2008 will be presented in the second part (Q. Ji et al., A novel nonintrusive method to resolve the thermal dome effect of pyranometers: 2. An application to surface radiative energetics, submitted to *Journal of Geophysical Research*, 2010).

2. Thermal Dome Effect

[5] There are a few key concerns regarding pyranometers, of which TDE is relatively complicated. Others include the cosine-response [e.g., *Collins*, 1966; *Michalsky et al.*, 1995] and the thermopile nonlinearity under extreme temperatures. All of these effects can be separated because the physical processes are independent. For example, the cosine-response remains relatively stable and it is not a function of temperature.

[6] The widely used pyranometers (e.g., Eppley model PSP, http://www.eppleylab.com) employ thermopiles as the detector for measuring the solar irradiance. The existence of TDE is evident, because even in the absence of solar irradiance, the thermopile still exhibits a nonzero output. This can be observed whenever a pyranometer operates in dark conditions, such as inside an enclosure, at nighttime, or by capping it [e.g., *Dutton et al.*, 2001; *Michalsky et al.*, 2003] during the day.

[7] Traditionally, pyranometer measurements are described as:

$$I_{\mathrm{h}} = c_{\mathrm{h}} V, \tag{1}$$

where V denotes the output voltage from the thermopile and c_{h} is a calibration constant. Notice that insufficient information is provided to correctly represent TDE. To properly account for TDE, at least two more pieces of information are needed: the case temperature (T_c) and the dome temperature (T_d), which functionally resembles a pyrgeometer, such as an Eppley model PIR for measuring infrared irradiance (note the PSP and PIR are similarly constructed, except that a PSP's double domes are transparent to solar radiation commonly in the 0.3–3 μm spectral range; while a PIR's smaller single dome is transmissive to terrestrial radiation frequently in the 4–50 μm range of infrared wavelengths).

[8] In order to collect sufficient information nonintrusively from a PSP, we slightly modified the instrument as illustrated in Figure 1. First, a thermistor is attached to the mounting plate of the thermopile to measure T_c. Second and innovatively, the space between the inner and the outer domes is sealed, and a pressure sensor (barometer) is used to measure the pressure of the trapped air (P_d). Consequently, T_d is known according to the ideal gas law:

$$P_d = rT_d, \tag{2}$$

where the gas coefficient, r, is ideally a constant that is proportional to the density of the trapped air. Equivalently, a constant-volume gas thermometer that fully covers the field of view of thermopile is created. Note that T_d does not represent the temperature at any particular point on the dome but rather is an effective-dome-temperature, i.e., what the thermopile senses in real-time from the overall thermal environment. Last, the air temperature (T_a) and pressure (P_a) are also monitored. Note, the thermopile's output voltage (V) and temperature (T_s, on the receiving surface of thermopile) are shown in the figure for reference.

[9] To investigate TDE in both laboratory and field studies, *Bush et al.* [2000] measured the temperatures of both the case and at a point on the outer dome of a pyranometer by attaching thermistors to the instrument. Through a linear fit of the measurements in dark conditions, they found the following relationship: $c_{\mathrm{h}}\ V = a\sigma(T_d^4 - T_c^4) + b$; where $a \approx 0.7$, σ is Stefan-Boltzmann constant, and $b \approx 0.08$ W m^{-2} is a small residual. This relationship was proposed for correcting a PSP's offset. A similar conclusion was also reached by *Haeffelin et al.* [2001] when they measured the temperatures of both the case and at a point on the inner dome of a pyranometer. Furthermore, based on the energy

balance in a pyranometer, *Ji and Tsay* [2000] showed that the measured solar irradiance, I, can be explicitly partitioned into two terms, one representing non-TDE which is strictly proportional to the output of the thermopile, and the other the TDE which is temperature dependent:

$$I = cV + f\sigma\left(T_s^4 - T_d^4\right), \tag{3}$$

where c, the intrinsic calibration constant, depends solely on the physical properties of instrument (e.g., shortwave reflectivity, emissivity of receiving surface, and thermopile sensitivity; note, it can also be a function of incident angle of irradiance, but should not be a function of temperature); f denotes a dome factor that mainly relies on the thermal emissivity of the dome; and T_s which is a function of two reliable measurements:

$$T_s = T_c + \alpha V, \tag{4}$$

where α is a constant converting an induced thermoelectric voltage (V) of the thermopile in response to a temperature difference (refer to Figure 1). Evidently, a TDE term is missing in equation (1); therefore TDE cannot be properly represented no matter how c_h is determined. From a different perspective, a variable TDE that depends on environmental conditions will be regarded as a constant and will be lumped into c_h during calibration. This makes the traditional calibration equation accurate only under the same conditions as at the time of calibration [*Ji*, 2007]. Consequently, the variable TDE is not accurately represented, leading to a "zero (or thermal) offset." From equations (3) and (4), $I \approx (c + 4 f \sigma \alpha T_c^3) V + f \sigma (T_c^4 - T_d^4) \approx c_h V + f \sigma (T_c^4 - T_d^4)$, which means that using c_h and T_c instead of c and T_s to partition the measurements will not isolate a non-TDE term [i.e., the $c V$ term in equation (3)], because even if the value of $(4 f \sigma \alpha T_c^3)$ is just a few percent of c, it makes c_h temperature dependent. Substituting equations (2) and (4) into (3), we obtain:

$$I = cV + f\sigma\left[(T_c + \alpha V)^4 - (P_d/r)^4\right]. \tag{5}$$

Thus, under ideal conditions, the resulting solar irradiance is derived from three trivial measurements (V, T_c and P_d) and five true constants (σ,α, r, plus c and f) that are rooted in stable physical properties.

3. Calibration Procedure

3.1. Ideal Conditions

[10] Ideally, finding the five constants in equation (5) is straightforward. First, $\sigma = 5.67 \times 10^{-8}$ W m^{-2} K^{-4}. Second, α can be deduced from the thermopile's physical properties (e.g., $\alpha = 694$ K V^{-1} [*Payne and Anderson*, 1999]). Third, r is determined by measuring a P_d under a known T_d. This can be done in a laboratory, or, a known T_d can be found in field measurements: $V = 0$ at night indicates that T_d reaches thermal equilibrium with T_c; in other words, whenever the thermopile does not sense a temperature difference while in dark conditions, $T_d = T_c$. Fourth, c and f form a pair similar to the counterpart used for the PIR, which can be determined [*Ji and Tsay*, 2000] by rearranging equation (5) as $I = c V + f D$, or:

$$I/D = cV/D + f, \tag{6}$$

where $D = \sigma [(T_c + \alpha V)^4 - (P_d/r)^4]$. Obviously, c and f are the slope and the offset respectively in a linear fit of (V/D) versus (I/D). Finally, a calibration standard, I, should be from a TDE-free reference.

3.2. Realistic Conditions

[11] Leaving the technical details of determining α to future studies, the value $\alpha = 694$ K V^{-1} is adopted in this paper. If α is slightly off by $\delta\alpha$, equation (5) becomes $I = c V + f \sigma [(T_c + (\alpha' - \delta\alpha) V)^4 - (P_d/r)^4] \approx c' V + f \sigma [(T_c + \alpha' V)^4 - (P_d/r)^4]$, where $\alpha' = \alpha + \delta\alpha$, and $c' \approx c - 4 f \sigma T_c^3 \delta\alpha$; in other words, the uncertainty in α will be lumped into c, which would be detectable because c is not supposed to be temperature dependent. The effect of the uncertainty can also be regarded as a repartition of the signal between the TDE term and the thermopile's direct response to solar radiation. As an estimation for a reasonably assumed condition: $c = 100$ W m^{-2} mV^{-1}, $f = 1$, and $T_c = 300$ K, an unreasonable 100% change of α may lead to about a 4% change in c. Since this change is balanced by the change in the TDE term, the measured irradiance is not significantly affected.

[12] Modifying a PSP can be straightforward and low cost; however, both the existing and added seals of the domes are not always ideal. Consequently, a small leak can cause r to gradually drift. However, c and f will not drift with a leak; therefore we can devise a two-part practical calibration procedure for finding these parameters, followed by determining the value of r dynamically.

[13] According to the ideal gas law, $\delta P_d = r\, \delta T_d + T_d\, \delta r$; in other words, a drift either in temperature or in gas coefficient can cause a change in pressure. Under a quasi-isothermal process $\delta T_d \approx 0$, therefore $\delta P_d \approx T_d\, \delta r$; which means that the outcome of a small leakage is a small change in pressure, and the leak can be measured by $\delta r \approx \delta P_d/T_d$. Technically δr can also be a result of thermal expansion, nevertheless only a leak is considered, because a PSP's coefficient of thermal expansion is at the 10^{-5} level, causing negligible effect to δP_d. Given that the leakage is between the confined volume and the atmosphere outside, the change of pressure is proportional to the pressure difference between them, i.e., $\delta P_d = k (P_d - P_a)$, where k is expected to be a slow varying coefficient for a small leak. This leads to $\delta r = k (P_d - P_a) / T_d$. By substituting $r = r_0 + \delta r$ into equation (2), we obtain:

$$P_d/T_d = r_0 + k(P_d - P_a)/T_d. \tag{7}$$

Obviously r_0 is the gas coefficient when $P_d = P_a$, and k is a gauge of the leak; or it can be regarded as a weighting factor between P_d and P_a, which is easily seen by rearranging equation (7) into $(1 - k) P_d + k P_a = r_0 T_d$. The parameters r_0 and k can be determined by a linear fit as long as they are relatively more stable than (P_d/T_d) and [($P_d - P_a$)/T_d], as demonstrated by our field measurements.

[14] T_d can be derived relying only on existing measurements. For example, from equations (3) and (4):

$$T_d = \left[(T_c + \alpha V)^4 + cV/(f\sigma)\right]^{1/4}, \text{ when } I = 0. \tag{8}$$

Table 1. Procedure to Determine c and f

Step	Action
1	Estimate nighttime T_d^{night} from equation (8) by assigning an initial value $c = c_h$ and a guess of f (normally $0 \le f \le 1$).
2	Use equation (7) on nighttime measurements to estimate r_0 and k.
3	Employ r_0 and k and apply equation (7) on daytime measurements to get T_d^{day}.
4	Substitute $D^{\text{day}} = \sigma\,[(T_c^{\text{day}} + \alpha\, V^{\text{day}})^4 - (T_d^{\text{day}})^4]$ into equation (6) to obtain a pair of c and f from daytime measurements.
5	If the difference between f and its initial guess is negligible then the correct values are found, otherwise update f and c, and repeat from Step 1.

Starting from this equation, the first part of the practical calibration procedure consists of five steps (Table 1) for finding c and f. The temperature versus pressure relationship determined at night can be extended to the daytime because the ideal gas law is not dependent on sunlight. Error propagations in the procedure can be estimated by introducing small perturbations δc and δf on top of the true values c_0 and f_0 respectively in equation (8). Following the procedure, this will alter the f determined by equation (6) into $f \approx f_0 + \beta\, f_0\, (\delta f/f_0 - \delta c/c_0)$, where $\beta = [(T_s^{\text{night}}/T_d^{\text{night}})^4 - 1]/[(T_s^{\text{day}}/T_d^{\text{day}})^4 - 1]$. At a typical temperature of 300 K, along with the thermopile's receiving surface warming by up to 5 K due to solar heating, and a 0.1 K temperature difference at night, $\beta = [(300.1/300)^4 - 1] / [(305/300)^4 - 1] \approx 0.02$. This indicates that the iterations in this part of the procedure will converge quickly, attributing to the distinct differences in thermal behavior between the pyranometer's nighttime and daytime operations.

[15] Once c and f are found, the second step in the practical calibration procedure for daily operations is to simply acquire r_0 and k from the nighttime measurements and to further derive T_d for the following (or the previous) day. Nevertheless, a perfect seal can be achieved and is preferred whenever affordable.

[16] In this procedure c and f are assumed to remain constant regardless of the incident angle of incoming irradiance, and daytime measurements are also used to determine the constants. In reality both c and f can weakly depend on the incident angle of incoming irradiance. Such issues and alternative ways for determining c and f can be investigated in future studies.

4. Data

[17] Among an array of instruments for remote sensing and in situ measurements (http://smartlabs.gsfc.nasa.gov/), a dozen of broadband radiometers to cover the global/direct/diffuse irradiances, and in different spectral bands were deployed in China during an Asian Monsoon Years (http://www.wcrp-amy.org/) field experiment in 2008. A modified PSP for this study was also tested. At Xianghe observatory (http://english/iap/cas.cn/rh/ss/), we collected data for nearly four months. The sampling rate was 1 Hz (Campbell Scientific CR7 data loggers, CR1000 for the modified PSP), and 1-min-averaged data are used in the following examples and discussions. Our broadband radiometers are calibrated routinely by BORCAL (National Renewable Energy Laboratory, http://www.nrel.gov/aim/borcal.html) based on the traditional calibration equation.

[18] As critical pieces of information, the three added measurements for the modified PSP are shown in Figure 2.

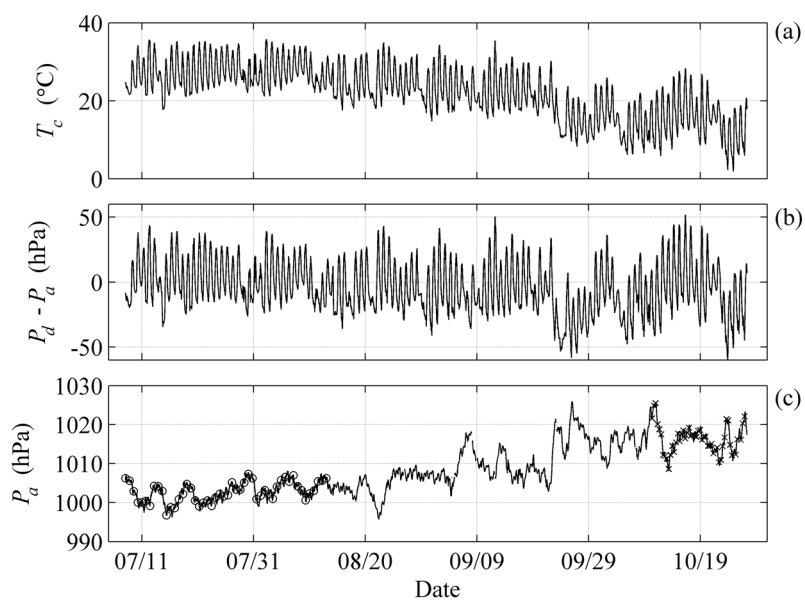

Figure 2. Added information measured over a nearly four-month period of (a) pyranometer's case temperature (T_c), (b) differential pressure between the sealed and outside air ($P_d - P_a$), and (c) outside air pressure (P_a). Note that collocated measurements from two additional barometers, depicted by the circles and crosses, are used to confirm the consistency of the measurements.

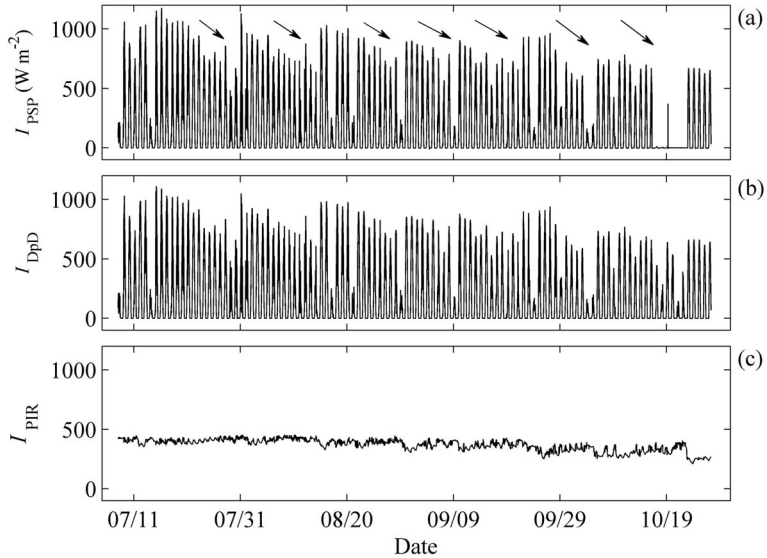

Figure 3. Measured solar and infrared irradiance from July through October by (a) the modified PSP (solar), (b) the DpD (solar), and (c) one of the PIRs (infrared). The arrows in Figure 3a indicate seven synoptic cycles we observed.

T_c (Figure 2a) was measured by a thermistor (0.1°C exchangeable) similar to those used in a PIR. It can be seen that the average daily temperature was around 30°C in early July, and dropped to around 10°C in late October; with a smaller daily variation under cloudy and rainy conditions. The pressure difference $P_d - P_a$ (Figure 2b) was measured by a silicon differential pressure sensor (uncertainty < 0.5 hPa). Notice that the daily swing of this differential pressure could be within 20 hPa or over 80 hPa depending on the environmental conditions. P_a (Figure 2c) was measured by a Vaisala weather transmitter (uncertainty < 0.5 hPa). An uncertainty of less than 0.5 hPa out of 1000 hPa translates into an uncertainty of less than 0.15°C in temperature out of 300 K, and into less than 0.9 W m^{-2} in blackbody thermal irradiance. This level of accuracy is achievable by using low cost data loggers such as the CR1000 (we normally use CR7 for higher accuracy and better resolution).

[19] Figure 3 is a glance of the relevant measurements from three collocated broadband radiometers over a period of 112 days. Figure 3a is the solar irradiance measurements (I_{PSP}) from our Eppley PSP, using the traditional calibration equation. The data gap (16–23 October) is from a test period in which the PSP was enclosed in a box to cut off the solar radiation. Figure 3b shows the combined direct and diffuse solar irradiance measurements from a pyrheliometer (Kipp&Zonen CH1) and shaded pyranometer (Kipp&Zonen CM21), respectively, i.e., the direct-plus-diffuse (DpD) components (I_{DpD}). There were also two collocated PIRs, which were not shaded unless sun-blocking clouds existed. In addition, one of them was not mechanically ventilated. Their measurement results differed slightly, but generally were within a few W m^{-2}. In Figure 3c are measurements from one of the PIRs (I_{PIR}), which showed a small diurnal variation, with an average of 367 W m^{-2} for the entire period. The three direct outputs from one of the PIRs are depicted in Figure 4. Its case temperature (T_{c_PIR}) is plotted in Figure 4a, while the differences between its dome temperature (T_{d_PIR}) and T_{c_PIR} are shown in Figure 4b. Unlike a PSP's clear dome, a PIR's opaque and smaller dome can become more than 1°C hotter than its case during the daytime, but can turn slightly cooler at night. Both T_{d_PIR} and T_{c_PIR} follow the trend of the PSP's T_c (Figure 2a); however, there are noticeable discrepancies because of the differences in the thermal characteristics of the two types of instrument. In addition to the seasonal decline and diurnal change, the synoptic variation is also evident in the broadband measurements (as indicated by the arrows in Figure 3a): after one or two rainy days, the solar irradiance was large during the following clean day and started to decrease (while the infrared irradiance increases) gradually over the next few days when pollutants and clouds built up. Hence, a diverse range of environmental conditions were experienced.

[20] The output of a PIR's thermopile is usually called the PIR's net-infrared-irradiance (NetIR), which is normally negative because the sky is cooler than the instrument, as shown in Figure 4c. This information can help to infer the PSP's TDE under certain assumptions. According to *Dutton et al.* [2001], the negative output from a pyranometer at night can be fitted by an "offset": $\Delta D_{IR} = b_0 + b_1$ NetIR + $b_2\ \sigma\ (T^4_{d_PIR} - T^4_{c_PIR})$; and the regression can be applied to the daytime measurements for correcting TDE. In other words, first this is the method that partitions solar irradiance into a traditionally calibrated part and an empirical NetIR correction part: $I = c_h\ V - \Delta D_{IR}$. Second the NetIR method utilizes four measurements from two collocated instruments: the output of PIR plus its case and dome temperatures in addition to the output of PSP.

5. Results and Discussions

5.1. The Missing Term in Traditional Calibration

[21] It is implied in the traditional calibration that $c_h\ V_{cal} = c\ V_{cal} + f\ D_{cal}$, in other words, $c_h = c + f\ D_{cal}/V_{cal}$, where D_{cal} and V_{cal} are the particular values happed at the moment

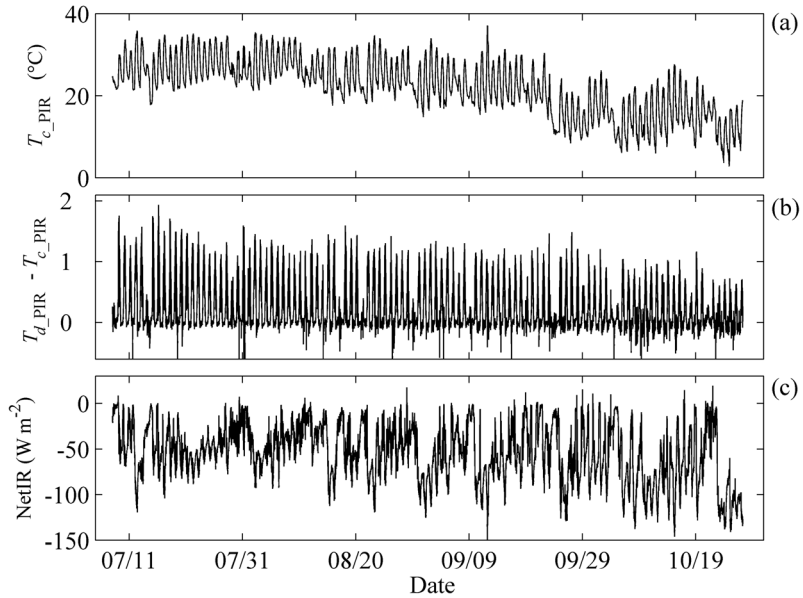

Figure 4. Measured PIR outputs, which are used for later comparisons with the new method, include (a) case temperatures (T_{c_PIR}), (b) temperature difference between dome and case ($T_{d_\mathrm{PIR}} - T_{c_\mathrm{PIR}}$), and (c) NetIR output from the PIR's thermopile.

of calibration, and are imbedded into the constant c_h. When equation (1) is used, a variable of $\delta I = I - I_\mathrm{h} = (c\ V + f\,D) - (c_\mathrm{h}\ V) = f\,[D - D_\mathrm{cal}\ (V/V_\mathrm{cal})]$ is not accounted for. The NetIR method is a practical way to infer this missing term, i.e., $\Delta D_\mathrm{IR} \approx -\,f\,[D - D_\mathrm{cal}\ (V/V_\mathrm{cal})]$.

[22] As an example to show the impact of this missing term, if a traditionally calibrated pyranometer is used as a calibration reference, then there should be $I^\mathrm{ref} - I_\mathrm{h}^\mathrm{ref} = f^\mathrm{ref}\,[D^\mathrm{ref} - D_\mathrm{cal}^\mathrm{ref}\ (V^\mathrm{ref}/V_\mathrm{cal}^\mathrm{ref})]$, where the superscript indicates that the values are from the reference pyranometer. By substituting I^ref into equation (6), we have:

$$I_h^\mathrm{ref}/D = \left[c + \left(f^\mathrm{ref} D_\mathrm{cal}^\mathrm{ref}/V_\mathrm{cal}^\mathrm{ref}\right)\left(V^\mathrm{ref}/V\right)\right] V/D + \left[f - f^\mathrm{ref}\left(D^\mathrm{ref}/D\right)\right] \approx c'V/D + f', \tag{9}$$

where c' and f' are the calibration constants to be determined by using the traditionally calibrated $I_\mathrm{h}^\mathrm{ref}$. How they will be affected by the uncertainties in the reference is revealed by equation (9). In addition, the cosine-response generally causes c to change slightly with solar elevation angle. If c is regarded as a constant regardless, then there will be a deviation of the value of f from the linear fit using equation (6) or (9). The outcome also depends on the range of irradiance used in calibration. Notice that the cosine-response effect and TDE are indistinguishable in the traditional calibration method.

[23] Nevertheless, it is recognized that DpD depends on the combined pyrheliometer and shaded pyranometer, in which the missing term caused by using the traditional calibration becomes smaller, therefore it exhibits less TDE and cosine-response effect [*McArthur*, 1998]. In this study we use the DpD as a reference to demonstrate the new method; however, in future studies rigorous calibrations will be performed using a true standard.

5.2. An Example of a Cloud-Free Day

[24] Relevant measurements from one of the cleanest days during the experiment period is presented in Figure 5. Figure 5a shows the infrared irradiance remained relatively unchanged during the course of the day, while the solar irradiance reached a maximum around noontime. It happens that the results from DpD during those few cloud-free days were noticeably lower than the uncorrected results from several collocated pyranometers including the modified PSP; nevertheless, we take the advantage to demonstrate how well the new calibration procedure can follow such a reference. Figure 5b clearly reveals that the temperature of the receiving surface of the PSP's thermopile can become several degrees hotter under solar radiation, while the temperatures on the case of the PSP, the PIR, and on the dome of the PIR all track each other closely. The discrepancy among all temperatures is usually less than a few tenth of a degree at night. Figure 5c shows that the air pressure remains relatively unchanged for the day, while the pressure of the air trapped between the PSP domes swings along with the temperatures. As shown in Figure 5d, large values of NetIR indicate clear sky conditions. In addition, there is a sizable increase in the NetIR during the daytime, and there is more variation compared to the night. This not only reflects the effect of solar heating to the instrument, but also indicates the difference between its daytime and nighttime thermal imbalance.

[25] The procedure listed in Table 1 for determining c and f is demonstrated step-by-step in Figure 6. The first step is to estimate the nighttime dome temperature using equation (8). In Figure 6a, T_d from the previous night (pluses) and following night (circles) are depicted. T_c is

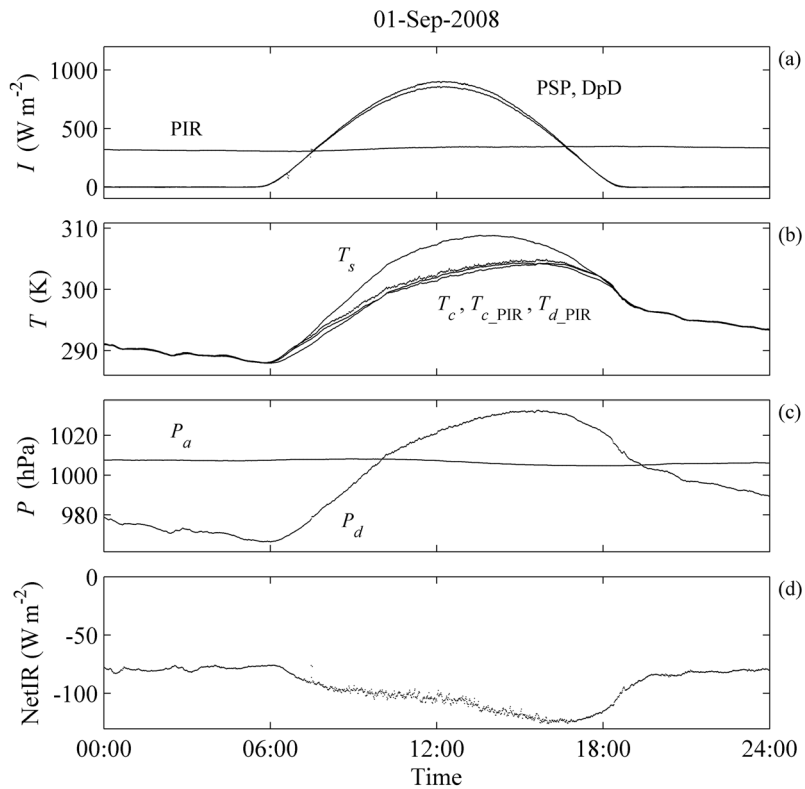

Figure 5. Measurements on a clean day showing (a) solar and infrared irradiances, (b) instrumental temperatures, (c) outside air pressure and the pressure of air trapped between the PSP domes, and (d) net-infrared irradiance from the PIR.

also shown in the background as a reference (gray curve). The second step (Figure 6b) is to apply the gas law in the form of equation (7) to obtain the pressure versus temperature relationship. Evidently, the close to unity coefficient-of-determination for the linear fitting (R^2 = 0.996) implies that equation (7) reliably captured the pressure versus temperature relationship. The third step (Figure 6c) is to derive the dome temperature during the daytime using the found relationship. The fourth step (Figure 6d) is to calculate the daytime D. The fifth step (Figure 6e) is to use equation (6) to determine c and f from the daytime measurements. To facilitate the comparison with the traditional calibration result, the ratio c/c_h is shown in Figure 6e instead of the value of c directly. The linear fit is based on those data points with both large solar elevation angle (>45°) and small change rate of temperature (<0.6 K h^{-1}). Note, the purpose of this presentation is to demonstrate the implementation of this procedure. It is not intended for rigorous calibration or quantitative comparison, because DpD is not a TDE-free calibration standard.

[26] Results of the aforementioned calibration procedure is depicted in Figure 7. Figure 7a shows the TDE term ($f\,D$, all positive values) along with a couple of corrections (ΔD_{IR}) derived using the NetIR method from the two collocated PIRs (the gray curve is from the PIR without mechanical ventilation). The instrument's case is normally warmer than its domes, which leads to $T_s > T_d$, and is thus a positive TDE term. There is a straightforward explanation for this: with solar radiation, the case receives more solar heating than the domes (broadband transparent in solar spectrum); without solar radiation and facing a colder sky, the case experiences less thermal cooling than the domes (opaque in infrared wavelengths). In addition, and less obvious, the case has a much larger thermal mass than the domes, therefore once the environmental temperature changes the case will lag behind, creating a temperature difference between the case and the domes, leading to an induced TDE. This will be further discussed later in section 5.5.

[27] A NetIR correction (ΔD_{IR}) is a patch to the traditional calibration results (c_h V); therefore, it depends on many details, such as when, where, and how the calibration was performed. Although the NetIR corrections from the two PIRs are virtually identical at night, they disagree with each other during the daytime. This is because each one of them has its own thermal characteristics, and its own relationship with the PSP. The large variations of ΔD_{IR} during the daytime are the result that a PIR's dome has a smaller thermal mass than that of the PSP's. A PIR's dome also experiences more solar heating (by direct and/or diffuse irradiance), therefore its temperature fluctuates more than the effective-dome-temperature of the PSP. This fluctuation does not affect the infrared irradiance measurement, because the PIR's own thermopile will see it and compensate for it. However, when used as a surrogate to infer the correction for a PSP's TDE, part of the fluctuations may be carried over unintended. This is one of the concerns of using an

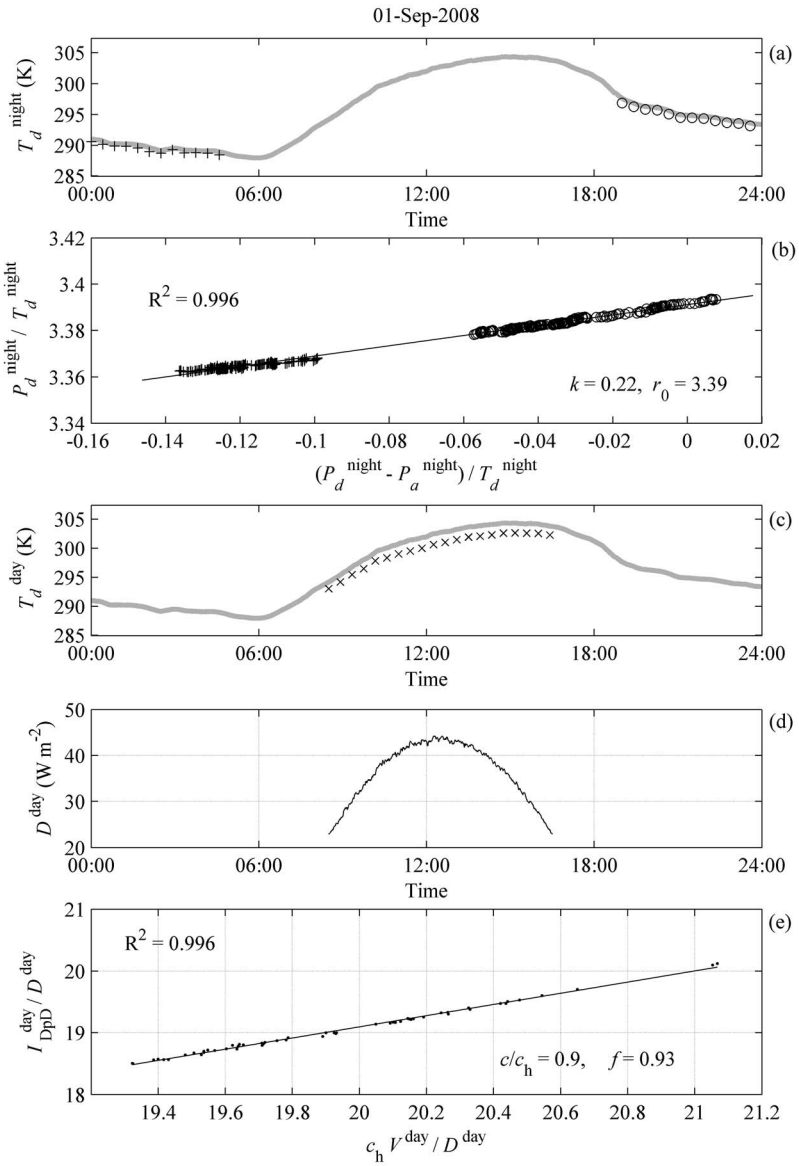

Figure 6. Example of calibration procedure for determining c and f on a clean day, following Table 1: (a) step 1, calculate nighttime dome temperature; (b) step 2, estimate r_0 and k from nighttime measurements; (c) step 3, derive the daytime dome temperature; (d) step 4, calculate the daytime D; and (e) step 5, determine c and f from the daytime measurements. The gray curve in Figures 6a and 6c is T_c.

indirect method. According to *Dutton et al.* [2001], the NetIR method is restricted to using a shaded PIR for the diffuse irradiance.

[28] Figure 7 also highlights the corrected irradiances at night and around noontime. At night (Figure 7c), three groups of curves can be clearly identified: the negative outputs of PSP before correction ($c_h V$) stay at the very bottom; directly above it in the middle are the negative outputs of DpD; and at the top around zero are the corrected results from the new method and the two NetIR corrections. Indeed, the negative outputs at night can be well compensated by both methods; however, their performances during the daytime are different. Around noontime (Figure 7b), there are also three groups of curves: the outputs of PSP before correction ($c_h V$) stay at the very top; the next two curves below it (one black, and the other gray) are the corrected results by the NetIR method using the two PIRs; and at the bottom, the curve from the new method overlaps with the curve for outputs of DpD, because the DpD is regarded as the reference target during calibration.

5.3. An Example of a Cloudy Day

[29] To illustrate how the new method works in a different environment, Figures 8, 9, and 10 resemble Figures 5, 6, and 7, respectively, except they are during cloudy conditions. Notice that the signals are noisier because of the inhomogeneity of clouds. Due to the difference in their ventilation, there were still noticeable discrepancies between the two

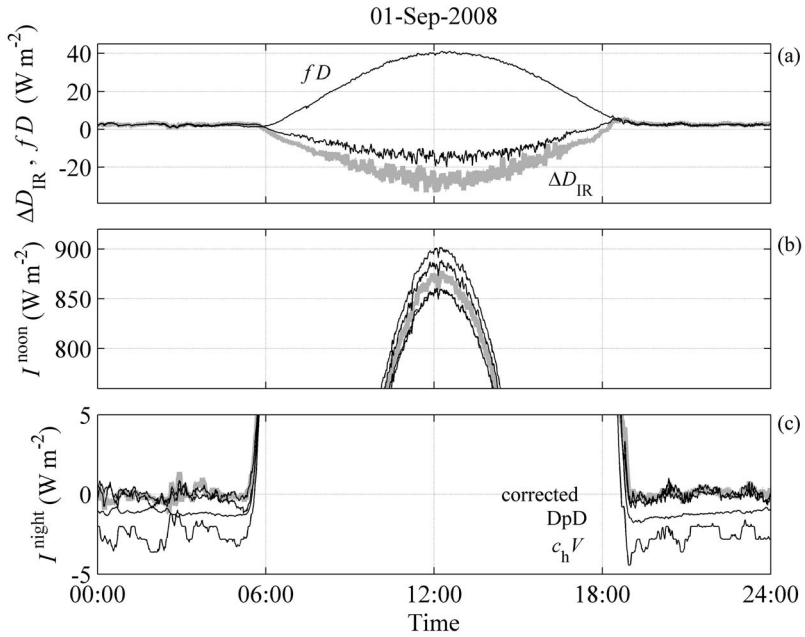

Figure 7. For clear day case, depicting (a) the captured TDE ($f\,D$) and the two NetIR corrections (ΔD_{IR}, black and gray curves), and the derived irradiances (b) around noontime and (c) at night. See section 5.2 for details.

NetIR corrections even if the two PIRs were shaded from the direct sun by clouds. The dependency of TDE on ventilation efficiency [e.g., *Ji*, 2007] makes the thermal issue more complex. However, since the TDE are directly obtained from the PSP, the new calibration method is less sensitive to ventilation or sky conditions. Figure 11 shows the available daytime data for determining c and f for both cloudy and cloud-free days, where the shade of the markers is assigned

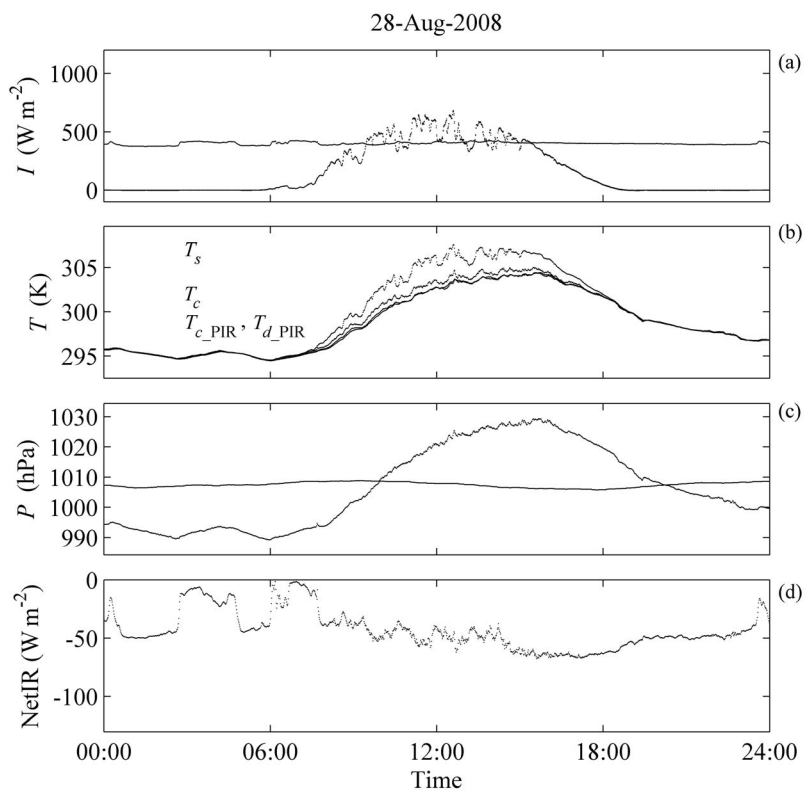

Figure 8. The same as Figure 5 but on a cloudy day.

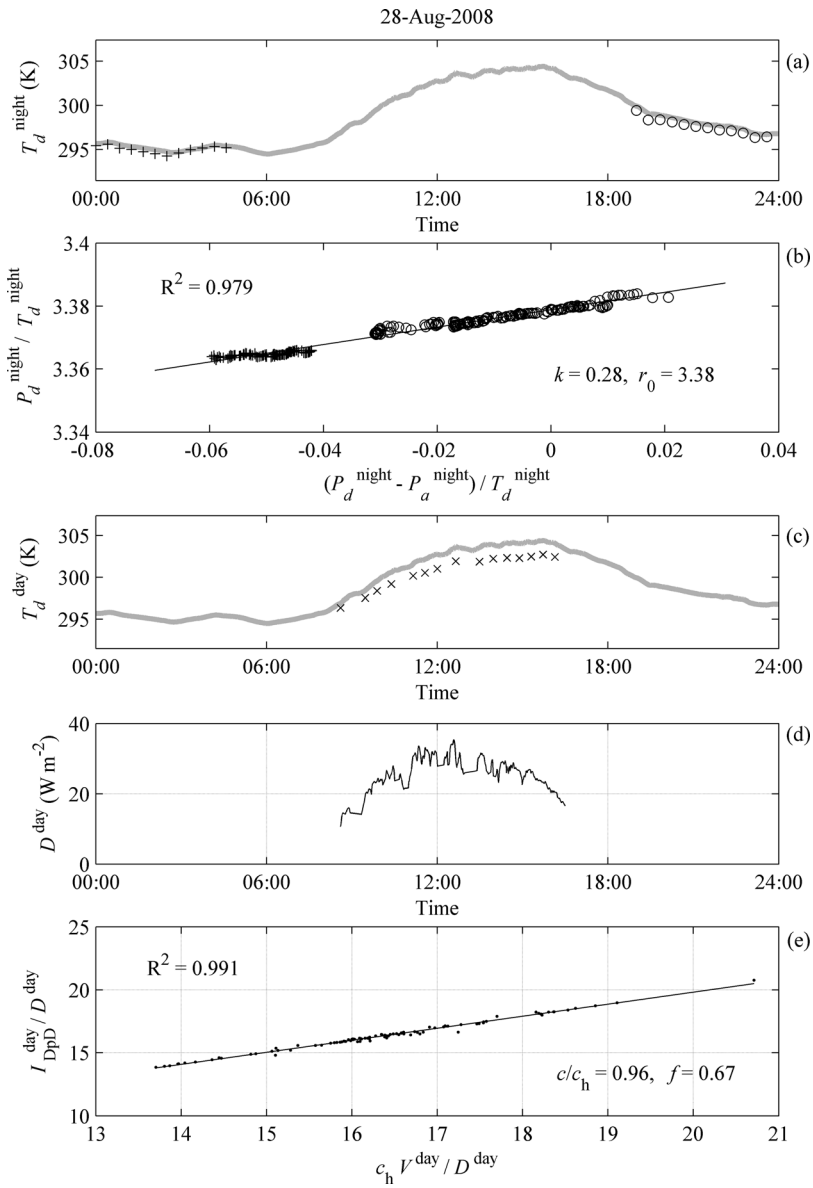

Figure 9. The same as Figure 6 but on a cloudy day.

according to the corresponding solar elevation angle of each data point. The data follow a linear fit better when the sun is blocked by clouds, indicating smaller cosine-response effect under cloudy condition.

[30] Following Figure 10a, Figure 12 shows a comparison of the directly captured TDE versus an indirectly inferred TDE (i.e., NetIR corrected irradiances scaled to match those from the DpD less the non-TDE part, or conceptually $c_h V - \Delta D_{IR} - c V$). Without a doubt they agree with each other reasonably well; however, the NetIR inferred values fluctuate more, and have a displacement – higher in the morning while the irradiance is rising, and lower in the afternoon when the irradiance is falling – compared to the results from the new method. This is due to the difference in PIR and PSP, which is clearly reflected in their temperature measurements (Figure 8b).

5.4. Long-Term Trend

[31] The trend of the effective-dome-temperature and TDE during the nearly four-month measurement period is demonstrated in Figure 13, where $c/c_h = 0.96$ and $f = 0.67$ are used in the calculation. Figure 13a highlights the first two days of three temperatures (T_s, T_c, and T_d). Notice that they are usually close to each other at night or under overcast/rainy conditions such as during the first day. The diurnal cycle and seasonal trend of T_c during the whole measurement period has been shown in Figure 2a. The differences of temperatures, $T_s - T_c$ and $T_d - T_c$, are shown in Figure 13b, which indicates that T_s is always higher than T_c during the daytime driven by solar radiation, but usually becomes slightly lower at night because of the combination of the direct thermal cooling of the domes plus the lagging behind of the case temperature during the drop of air temperature.

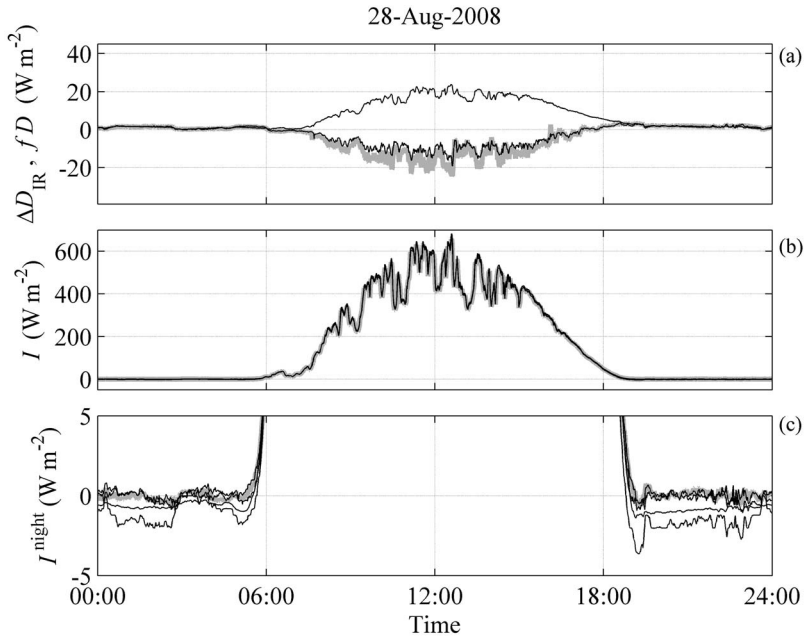

Figure 10. The same as Figure 7 but for cloudy case. Notice the TDE is smaller compared to that under the cloud-free conditions.

Additionally, T_d is usually lower than T_c, except during rainy periods; or when the PSP is in an enclosure, whereby the direct thermal cooling to the cold sky is cut off, and the thermal heating from the enclosure and the lagging of T_c behind T_d remain the major components. The captured TDE is shown in Figure 13c, which is usually positive and can reach over 30 W m^{-2} around noontime; however, it can become negative during rainy periods, or whenever $T_s < T_d$ occurs. Obviously the TDE follows the sky conditions, which can be seen by comparing to the irradiance measurements (see

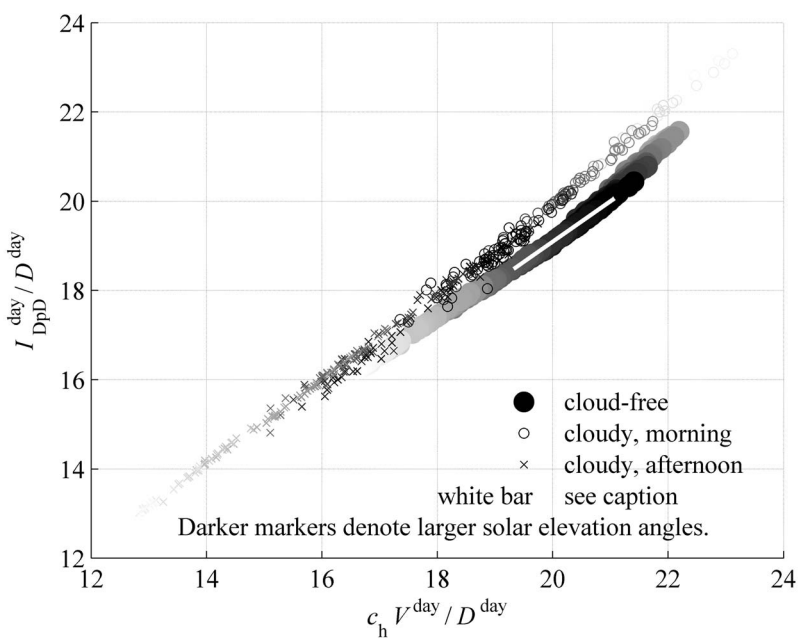

Figure 11. Selection of data for calibration. The daytime data with a solar elevation angle larger than 25° are shown, where darker markers denote larger angles (which reached up to 60°). The solid dots are for the cloud-free case. The white bar in the center is the same as the fit line shown in Figure 6e, which corresponds to the data when the solar elevation angle was larger than 45°, and the change rate of temperature was smaller than 0.6 K h^{-1}. The open circles and the crosses are for the cloudy case, in the morning and in the afternoon, respectively. The effect of solar elevation is less pronounced when it is cloudy.

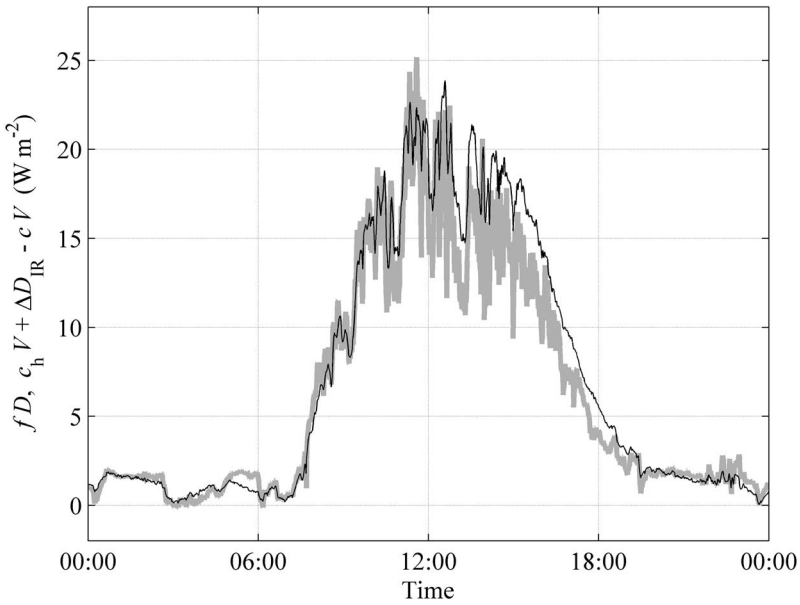

Figure 12. Comparison of the TDE captured on the PSP (black curve) and a NetIR inferred one (gray curve). Note the latter curve fluctuates more and has a displacement during the daytime compared to that from the former one (black curve). This is due to the differences in the thermal characteristics of PIR and PSP.

Figure 3). The derived daily r_0 and k are shown in Figure 14. Following the gas law, r_0 drifted slowly with air pressure (see Figure 2) and temperature. Finally, k remained around 0.2 during the measurement period, indicating that our low cost modification to the PSP held up reasonably well.

5.5. TDE Due to Temperature Variations

[32] Following the discussion in section 5.2, how the change of temperature causes TDE is clearly revealed in Figure 15. A test can be done by placing the PSP inside an enclosure, where temperature is the only concern in absence of solar radiation. Obviously, the induced TDE is proportional to the change rate of temperature, i.e., the faster the temperature changes, the more T_c lags behind T_d, and the larger the TDE (solid dots). This lagging effect, or the effect of differential thermal mass between case and domes, can also be seen in the daily trend of the negative nighttime output of the PSP, which tends to become smaller before

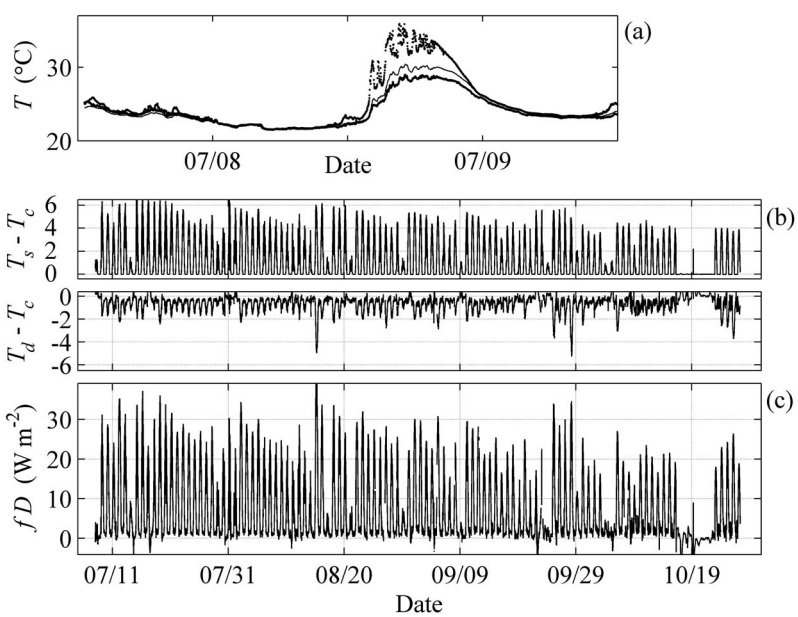

Figure 13. (a) Highlights of the first two days of T_s, T_c, and T_d (top, middle, and bottom curves, respectively). For the whole measurement period, (b) $T_s - T_c$ is mostly positive and can be larger than 6°C while $T_d - T_c$ is usually negative and within −2°C and (c) fD (i.e., TDE) varies with T_s and T_d.

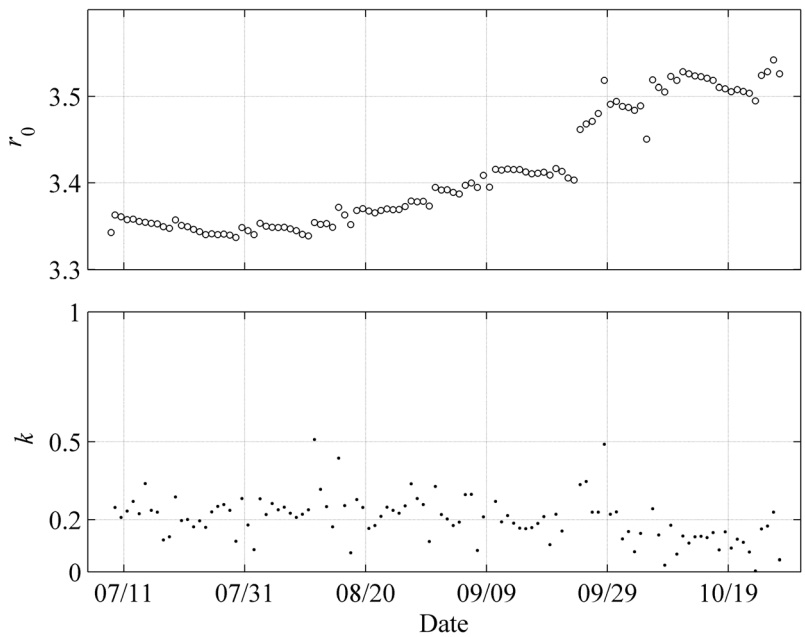

Figure 14. Derived daily r_0 and k over the same measurement period. Note that for ideal condition (i.e., domes are perfectly sealed), r_0 stays constant and k is zero.

dawn when the change rate of air temperature is smaller. This type of TDE also depends on how well the case can catch up with the domes, i.e., at a given change rate of temperature, the narrower the gap between T_c and T_d, the smaller the TDE. In Figure 15, the cluster with smaller slope (circles) is from the period when the PSP was better insulated (wrapped in thick layers of foam) that helped the case and the domes to pursue thermal equilibrium easier. Efficient ventilation may serve the same purpose. Naturally, the induced TDE becomes zero if there is no change in tem-

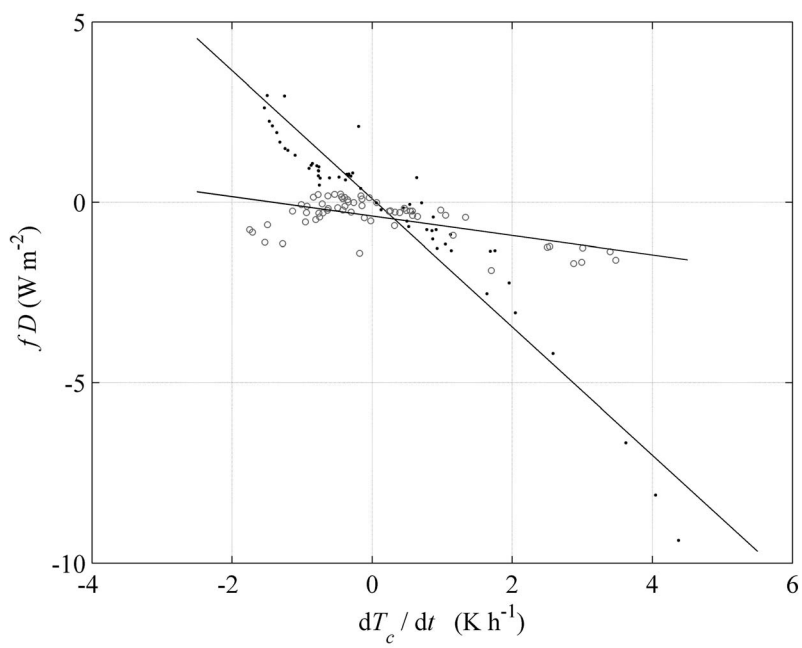

Figure 15. Induced TDE from environmental temperature changes, derived from the modified PSP inside an enclosure. Because of differences in the dome's and case's thermal masses, the faster the environmental temperature changes, the more the case temperature lags behind the dome temperature, and the larger the induced TDE (larger slope – solid dots). With better insulation, the dome and case temperatures will follow each other more closely, resulting in a smaller TDE (smaller slope – gray circles). See section 5.5 for further discussion.

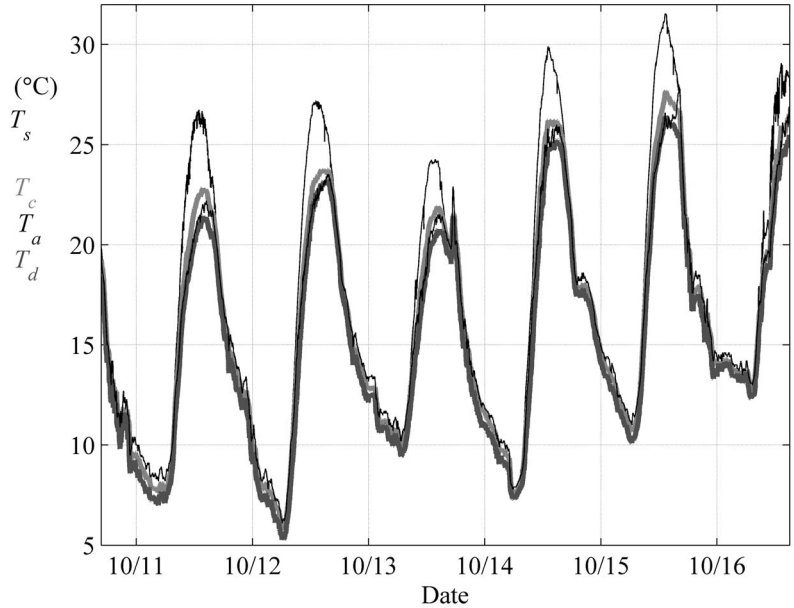

Figure 16. Under solar radiation the receiving surface of the thermopile can become over 5°C hotter (T_s, black curve on top), while the case (T_c) and dome (T_d) temperatures (both gray curves) follow the air temperature (T_a, black curve overlapped with gray curves) closely, thus offering the potential for correcting historical data. See section 5.7 for details.

perature, or if T_c could follow T_d instantaneously. To avoid this extra TDE, only the data during the period when the temperature changed slower than 0.6°C per hour were used for calculations in the demonstration shown in sections 5.2 and 5.3.

[33] An example of allowing the case to better follow the domes thermally comes from a Kipp&Zonen CM21. A CM21 is made with a smaller thermal mass (aluminum instead of copper, and smaller size) than a PSP, in addition of a better thermal contact between dome and case (thicker glass) and stronger ventilation (larger fan). Another example is a pyrheliometer, such as the Eppley NIP and Kipp&Zonen CH1. Their thermal masses are relatively small, plus the dome occupies only a small portion of detector's field of view, resulting in a smaller negative output at night than those from a PSP. Finally, the nighttime outputs of an Eppley B/W pyranometer is almost zero, serving as an example of when T_c could follow T_d instantaneously. Due to the B/W's special construction, its detector is a differential thermopile with both the hot junction (blackened) and the cold junction (whitened) exposed to the same thermal environment facing the dome, therefore theoretically equation (4) becomes $T_s = T_d + \alpha V$ for a B/W. With T_c out of the equation, the induced TDE by T_c lagging behind T_d during temperature change is eliminated. Consequently, the B/W's measurements become $I = c V + f \sigma [(T_d + \alpha V)^4 - (T_d)^4] \approx c V + (4 f \sigma \alpha T_d{}^3) V$. This reveals that although TDE diminishes at night or in a cap test (when $V \approx 0$), the B/W's TDE term is not negligible during daytime. Similarly, the negative output seen in a cap test on a PSP is not its true TDE. Because when solar radiation is blocked, the receiving surface of the thermopile is no longer heated, and its temperature swiftly drops several degrees, resulting in a change of the thermal imbalance. In addition, a cap does not just block the solar radiation; it also alters the thermal environment by letting the dome view in the infrared a much hotter target instead of the cold sky. It is also revealed that adding ventilation may help to stabilize B/W's TDE by reducing the fluctuations in its T_d.

5.6. Cost Advantage of the New Method

[34] Compared to existing methods, the new method is a cost effective way to account for TDE. For example, reducing the thermal mass of the instrument or improving thermal contact between the dome and the case is neither a low-cost modification nor a TDE-free solution. Also, measuring the direct solar and the shaded diffuse sky irradiances separately will reduce, but not fully account for TDE. A dome-less active cavity type of high precision instrument can be used to replace a pyrheliometer, but it is expensive and not suitable for daily operation. Moreover, the additional costs of a solar tracker and a pyrheliometer is many times over that of a pyranometer. Finally, the NetIR method requires a collocated pyrgeometer, which costs more than a pyranometer.

5.7. Potential for Correcting Historical Pyranometer Measurements

[35] As mentioned previously, TDE cannot be fully accounted for no matter how c_h is derived, because the dynamics of the effective-dome-temperature cannot be represented by equation (1) as long as c_h is a constant. Currently a possible approach for correcting historical pyranometer measurements is the NetIR method, if the collocated pyrgeometer measurements are available. In that case the TDE is regarded to be indirectly measured under certain assumptions. Alternatively, the auxiliary data most likely available for serving as a surrogate is air temperature, T_a. The assumption is that the ventilation of a pyranometer

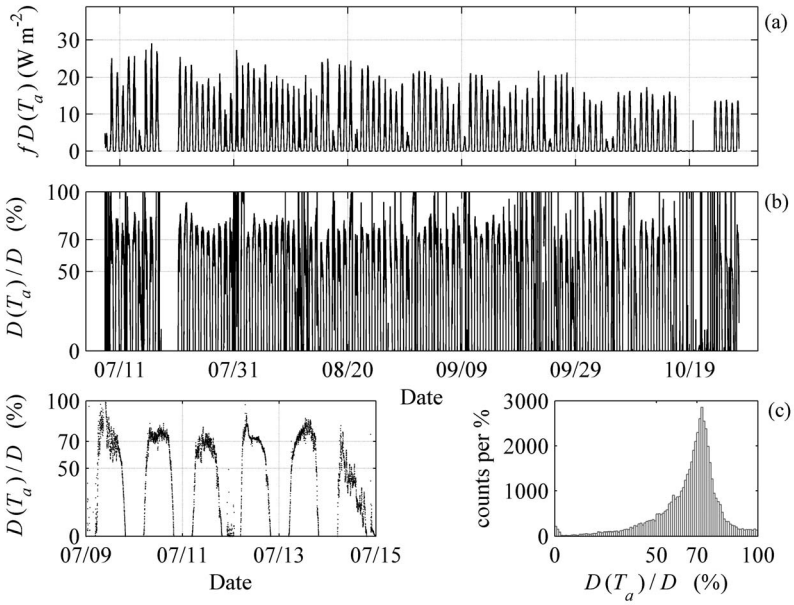

Figure 17. (a) An example of estimating TDE by using air temperature as a surrogate, in which (b) about 70% of the TDE can be captured during the measurement period, with details for (c) (left) the first few days and (right) the histogram from all daytime ratios during the nearly 4-month period.

(whether by natural or artificial means) was sufficient to keep the temperatures of the case and domes close to that of the surrounding atmosphere. According to equations (3) and (4), using T_a as a surrogate will lead to $I(T_a) = c\ V + f\ D(T_a) = c\ V + f\ \sigma\ [(T_a + \alpha\ V)^4 - T_a^4] \approx (c + 4\ f\ \sigma\ \alpha\ T_a^3)\ V$. This can be regarded as a partial correction of the temperature effect to c_h, and making it a variable. A major portion of the daytime TDE can be quantified, because the difference between T_s and T_c is usually much larger than the difference between T_c and T_a (see Figure 16). This is demonstrated in Figure 17 where most of the time about 70% of TDE can be accounted for. The result depends on the environmental and instrumental conditions, which deserves further investigation.

6. Conclusions and Future Work

[36] We devised a new technique to measure the effective-dome-temperature directly and nonintrusively from a pyranometer. Together with the case temperature, this provides a crucial piece of information for determining the thermal dome effect of a pyranometer, thus reducing the uncertainty of solar irradiance measurements. A procedure to use the added information has also been demonstrated. Specifically, by applying the ideal gas law, the effective-dome-temperature is derived by measuring the pressure of air sealed between the inner and outer domes. In addition, the measured irradiance is partitioned explicitly into a non-TDE term and a TDE term. Unlike other methods that have been proposed and/or in operations, this new method relies on measurements of stable physical coefficients directly from the same pyranometer without affecting its optical and thermal properties. Its cost-effectiveness is unlikely to be succeeded by any other known methods that target on reducing and/or inferring TDE.

[37] By incorporating additional information, the new method is more accurate than the traditional method. This will help to upgrade operational pyranometers for conducting climate-quality measurements. Planning of a mini DOE/ARM Intensive Observation Period following the work of *Michalsky et al.* [2003, 2005] is underway for intercomparison and further improvements.

[38] **Acknowledgments.** This research is supported by NASA's Radiation Science Program, managed by Hal B. Maring. We sincerely thank Warren J. Wiscombe for his in-depth comments and suggestions. We are also grateful to Thomas Stoffel and his team at NREL for calibration of our radiometers, Hongbin Chen and his team at IAP for help during the deployment at Xianghe observatory, and Richard A. Hansell for comments and suggestions.

References

Bush, B. C., F. P. J. Valero, and A. S. Simpson (2000), Characterization of thermal effects in pyranometers: A data correction algorithm for improved measurement of surface insolation, *J. Atmos. Oceanic Technol.*, *17*, 165–175, doi:10.1175/1520-0426(2000)017<0165:COTEIP>2.0.CO;2.

Collins, B. G. (1966), Determination of the cosine response of pyranometers, *J. Sci. Instrum.*, *43*, 837–838, doi:10.1088/0950-7671/43/11/416.

Dutton, E. G., J. J. Michalsky, T. Stoffel, B. W. Forgan, J. Hickey, D. W. Nelson, T. L. Alberta, and I. Reda (2001), Measurement of broadband diffuse solar irradiance using current commercial instrumentation with a correction for thermal offset errors, *J. Atmos. Oceanic Technol.*, *18*, 297–314, doi:10.1175/1520-0426(2001)018<0297:MOBDSI>2.0.CO;2.

Gulbrandsen, A. (1978), On the use of pyranometers in the study of spectral solar radiation and atmospheric aerosols, *J. Appl. Meteorol.*, *17*, 899–904, doi:10.1175/1520-0450(1978)017<0899:OTUOPI>2.0.CO;2.

Haeffelin, M., S. Kato, A. M. Smith, K. Rutledge, T. Charlock, and J. R. Mahan (2001), Determination of the thermal offset of the Eppley Precision Spectral Pyranometer, *Appl. Opt.*, *40*, 472–484, doi:10.1364/AO.40.000472.

Intergovernmental Panel on Climate Change (2007), Climate change 2007: Synthesis report, 103 pp., Geneva, Switzerland. (Available at http://www.ipcc.ch/pdf/assessment-report/ar4/syr/ar4_syr.pdf)

Ji, Q. (2007), A method to correct the thermal dome effect of pyranometers in selected historical solar irradiance measurements, *J. Atmos. Oceanic Technol.*, *24*, 529–536, doi:10.1175/JTECH1977.1.

Ji, Q., and S.-C. Tsay (2000), On the dome effect of Eppley pyrgeometers and pyranometers, *Geophys. Res. Lett.*, *27*(7), 971–974, doi:10.1029/1999GL011093.

McArthur, L. J. B. (1998), *Baseline Surface Radiation Network (BSRN) operations manual*, *WMO/TD-879*, 69 pp., World Clim. Res. Program, Geneva, Switzerland.

Michalsky, J. J., L. C. Lee, and W. E. Berkheiser III (1995), Cosine response characteristics of some radiometric and photometric sensors, *Sol. Energy*, *54*, 397–402, doi:10.1016/0038-092X(95)00017-L.

Michalsky, J. J., et al. (2003), Results from the first ARM diffuse horizontal shortwave irradiance comparison, *J. Geophys. Res.*, *108*(D3), 4108, doi:10.1029/2002JD002825.

Michalsky, J. J., et al. (2005), Toward the development of a diffuse horizontal shortwave irradiance working standard, *J. Geophys. Res.*, *110*, D06107, doi:10.1029/2004JD005265.

Payne, R. E., and S. P. Anderson (1999), A new look at calibration and use of Eppley precision infrared radiometers. Part II: Calibration and use of the Woods Hole Oceanographic Institution improved meteorology precision infrared radiometer, *J. Atmos. Oceanic Technol.*, *16*, 739–751, doi:10.1175/1520-0426(1999)016<0739:ANLACA>2.0.CO;2.

Philipona, R. (2002), Underestimation of solar global and diffuse radiation measured at Earth's surface, *J. Geophys. Res.*, *107*(D22), 4654, doi:10.1029/2002JD002396.

Reda, I., T. Stoffel, and D. Myers (2003), A method to calibrate a solar pyranometer for measuring reference diffuse irradiance, *Sol. Energy*, *74*, 103–112, doi:10.1016/S0038-092X(03)00124-5.

Stephens, G. L., and S. C. Tsay (1990), On the cloud absorption anomaly, *Q. J. R. Meteorol. Soc.*, *116*, 671–704, doi:10.1002/qj.49711649308.

World Meteorological Organization (2008), Guide to meteorological instruments and methods of observation, 7th ed., *WMO-8*, Geneva, Switzerland.

Q. Ji and S.-C. Tsay, ESSIC, Code 613.2, NASA Goddard Space Flight Center, MD 20771, USA. (qiang.ji-1@nasa.gov)